

Inclusive Gluon Production in Pion-Proton Collisions and the Role of Infrared Renormalons

A. I. Ahmadov^{1 *}, C. Aydin^{2 †}, R. Myrzakulov^{3 ‡}, and O. Uzun^{2 §}

¹ *Department of Theoretical Physics, Baku State University,
Z. Khalilov st. 23, AZ-1148, Baku, Azerbaijan*

² *Department of Physics, Karadeniz Technical University, 61080, Trabzon, Turkey and*

³ *Eurasian International Center for Theoretical Physics
and Department of General Theoretical Physics,
Eurasian National University, Astana 010008, Kazakhstan*

(Dated: June 9, 2019)

Abstract

In this article we calculate the contribution of the higher-twist Feynman diagrams to the large- p_T inclusive gluon production cross section in πp collisions in case of the running coupling and frozen coupling approaches within perturbative and holographic QCD. We obtain the structure of infrared renormalon singularities of the higher-twist subprocess cross section. We also compared and analyzed the resummed higher-twist cross sections (Borel sum) with the ones obtained in the framework of the frozen coupling approach and leading-twist cross section.

PACS numbers: 12.38.-t, 13.60.Le, 14.40.Aq, 13.87.Fh

Keywords: higher-twist, pion distribution amplitude, infrared renormalons

* E-mail: ahmadovazar@yahoo.com

† E-mail: coskun@ktu.edu.tr

‡ E-mail: rmyrzakulov_@gmail.com

§ E-mail: oguzhan_deu@hotmail.com

I. INTRODUCTION

It is well known that Quantum chromodynamics (QCD) is the fundamental theory of the strong interactions. Many researchers study QCD to describe the structure and dynamical properties of hadrons at the amplitude level. The hadronic distribution amplitude in terms of internal structure degrees of freedom is important in QCD process predictions.

One of the basic problems QCD is choosing the renormalization scale in running coupling constant $\alpha_s(Q^2)$. In principle, that in perturbative QCD (pQCD) calculations, the argument of the running coupling constant in both the renormalization and factorization scale Q^2 should be taken equal as to the square of the momentum transfer of a hard gluon in a corresponding Feynman diagram [1].

In the perturbative QCD, the physical information of the inclusive gluon production is obtained efficiently; therefore, it can be directly compared to the experimental data.

The main aim of this study calculation and analysis inclusive gluon production in the pion-proton collisions using the frozen and running coupling constant approaches.

Using the frozen and running coupling constant approaches the higher twist effects were already calculated by many authors [2–15].

The calculation and analysis of the higher-twist effects on the dependence of the pion distribution amplitude in inclusive gluon production at πp collision within holographic and pQCD approaches are one of the interesting research problem. In our former study, using the principle of maximum conformality and Brodsky-Lepage-Mackenzie (BLM) approaches, we have calculated the contribution of the higher-twist mechanism to the large- p_T inclusive gluon production cross section in πp collisions [12]. In this work we computed the contribution of the higher-twist effects to an inclusive gluon production cross section by using various pion distribution amplitudes from holographic and perturbative QCD applying the frozen and running coupling constant approaches.. We have also estimated and performed comparisons of the leading and the higher-twist contributions.

Detailed studying various properties of the hadron infrared renormalon effects is one of the essential and actual problems in the perturbative QCD [16–21]

In this study, we apply the running [22] and frozen coupling approaches in order to compute the effects of the infrared renormalons on the inclusive gluon production at πp collision within holographic and pQCD. This approach was also employed before [5–11] to

calculate the inclusive meson production in pp and $\gamma\gamma$ collisions.

The paper is planned as follows. The formulae for the calculation of the contributions of the higher-twist and leading-twist diagrams are provided in Section II. Some formulae and analysis of the higher twist effects on the dependence of the pion distribution amplitudes by the running coupling constant approach is presented in Section III, and the numerical results for the cross section and discussion of the dependence of the cross section on the pion distribution amplitudes are presented in Section IV. Finally, our conclusions and the highlights of the study are listed in Sec. V.

II. HIGHER-TWIST AND LEADING-TWIST CONTRIBUTIONS TO INCLUSIVE GLUON PRODUCTION

The higher-twist Feynman diagrams for the inclusive gluon production in the pion-proton collision $\pi p \rightarrow gX$ are shown in Fig.1. The amplitude for this subprocess is found by means of the Brodsky-Lepage formula [23]

$$M(\hat{s}, \hat{t}) = \int_0^1 dx_1 \int_0^1 dx_2 \delta(1 - x_1 - x_2) \Phi_M(x_1, x_2, Q^2) T_H(\hat{s}, \hat{t}; x_1, x_2) \quad (2.1)$$

where T_H is the sum of the graphs contributing to the hard-scattering part of the subprocess. For the higher-twist, the subprocess $\pi q_p \rightarrow gq$ is taken, which contributes to $\pi p \rightarrow gX$, where q_p is a constituent of the initial proton target. As seen from Fig.1, processes $\pi^+ p \rightarrow gX$ and $\pi^- p \rightarrow gX$ arise from subprocesses as $\pi^+ d_p \rightarrow gu$ and $\pi^- u_p \rightarrow gd$, respectively.

The production of the hadronic gluon in the large transverse momentum is available at the high energy, especially at the Large Hadron Collider. Hadronic gluon as final are a product of the hard-scattering processes, before hadronization. In the final state this hadronic gluon is fragmented to hadron. The main dynamical properties of the gluon is close to the parent parton, which carried one of the part four momentum of parent parton. In order to understand the parton kinematics one should consider the gluon production process [24].

The higher-twist cross section for $\pi p \rightarrow gX$ process has the form:

$$E \frac{d\sigma}{d^3p}(\pi p \rightarrow gX) = \int_0^1 dx \delta(\hat{s} + \hat{t} + \hat{u}) \hat{s} G_{q/p}(x, Q^2) \frac{1}{\pi} \frac{d\sigma}{d\hat{t}}(\pi q_p \rightarrow gq), \quad (2.2)$$

where $G_{q/p}(x, Q^2)$ is the quark distribution function inside a proton.

The Mandelstam invariant variables for higher-twist subprocess $\pi q_p \rightarrow gq$ we can write in the form:

$$\hat{s} = (p_1 + p_g)^2 = (p_2 + p_\pi)^2, \quad \hat{t} = (p_g - p_\pi)^2, \quad \hat{u} = (p_1 - p_\pi)^2. \quad (2.3)$$

and from [25]

$$\frac{d\sigma}{d\hat{t}}(\pi q_p \rightarrow gq) = \frac{256\pi^2}{81\hat{s}^2} [D(\hat{s}, \hat{u})]^2 \left(-\frac{\hat{t}}{\hat{s}^2} - \frac{\hat{t}}{\hat{u}^2} \right), \quad (2.4)$$

where

$$D(\hat{s}, \hat{u}) = \int_0^1 dx \alpha_s^{3/2}(Q_1^2) \left[\frac{\Phi_\pi(x, Q_1^2)}{x(1-x)} \right] + \int_0^1 dx \alpha_s^{3/2}(Q_2^2) \left[\frac{\Phi_\pi(x, Q_2^2)}{x(1-x)} \right], \quad (2.5)$$

here $Q_1^2 = (1-x)\hat{s}$ and $Q_2^2 = -x\hat{u}$ represent the momentum square of the hard gluon in Fig.1.

There are few forms of pion distribution amplitude available in the literature. In the present numerical calculations, we used several choices, such as the asymptotic distribution amplitude derived in pQCD evaluation [26], the Vega-Schmidt-Branz-Gutsche-Lyubovitskij (VSBGL) distribution amplitude [27], distribution amplitudes predicted by AdS/CFT [28, 29], and the Chernyak-Zhitnitsky(CZ) [30], the Bakulev-Mikhailov-Stefanis (BMS) [31] and pion distribution amplitudes, which Gegenbauer coefficients a_2 and a_4 extracted from BELLE experiment [32]:

$$\Phi_{asy}(x) = \sqrt{3}f_\pi x(1-x), \quad (2.6)$$

$$\Phi_{VSBGL}^{hol}(x) = \frac{A_1 k_1}{2\pi} \sqrt{x(1-x)} \exp\left(-\frac{m^2}{2k_1^2 x(1-x)}\right), \quad (2.7)$$

$$\Phi^{hol}(x) = \frac{4}{\sqrt{3}\pi} f_\pi \sqrt{x(1-x)}, \quad (2.8)$$

$$\Phi_{CZ}(x, \mu_0^2) = \Phi_{asy}(x) \left[C_0^{3/2}(2x-1) + \frac{2}{3}C_2^{3/2}(2x-1) \right], \quad (2.9)$$

$$\Phi_{BMS}(x, \mu_0^2) = \Phi_{asy}(x) \left[C_0^{3/2}(2x-1) + 0.20C_2^{3/2}(2x-1) - 0.14C_4^{3/2}(2x-1) \right], \quad (2.10)$$

$$\Phi_{BELLE}(x, \mu_0^2) = \Phi_{asy}(x) \left[C_0^{3/2}(2x-1) + 0.12C_2^{3/2}(2x-1) + 0.08C_4^{3/2}(2x-1) \right], \quad (2.11)$$

here $C_n^\lambda(2x-1)$ are Gegenbauer polynomials.

If we put Eq.(2.4) into Eq.(2.2) then differential cross section for the process $\pi p \rightarrow gX$ is written as

$$E \frac{d\sigma}{d^3p}(\pi p \rightarrow gX) = \frac{s}{s+u} x G_{q/p}(x, Q^2) \frac{256\pi}{81\hat{s}^2} [D(\hat{s}, \hat{u})]^2 \left(-\frac{\hat{t}}{\hat{s}^2} - \frac{\hat{t}}{\hat{u}^2} \right). \quad (2.12)$$

It should be noted that, as seen from Eq.(2.4) and Eq.(2.13), the higher-twist cross section is linear with respect to \hat{t} , so the cross section is identical to zero, if the scattering angle between the final gluon and incident pion is approximately equal to zero, $\theta = 0$. From Eq.(2.13) is seen that, higher-twist cross section proportional to \hat{s}^{-3} , it is equivalently that higher-twist contributions to the $\pi p \rightarrow gX$ cross section have the form of $p_T^{-6} f(x_F, x_T)$.

Despite this, the extracting of higher-twist contribution from the inclusive gluon production cross section is complicated. One can also consider the comparison of higher-twist corrections with leading-twist contributions. For the leading-twist subprocess in the inclusive gluon production, we take $q\bar{q} \rightarrow g\gamma$ as a subprocess of the quark-antiquark annihilation. The differential cross section for subprocess $q\bar{q} \rightarrow g\gamma$ is

$$\frac{d\sigma}{d\hat{t}}(q\bar{q} \rightarrow g\gamma) = \frac{8}{9}\pi\alpha_E\alpha_s(Q^2)\frac{e_q^2}{\hat{s}^2}\left(\frac{\hat{t}}{\hat{u}} + \frac{\hat{u}}{\hat{t}}\right). \quad (2.13)$$

The leading-twist cross section for production of inclusive gluon is [33]

$$\Sigma_M^{LT} \equiv E \frac{d\sigma}{d^3p}(\pi p \rightarrow gX) = \int_0^1 dx_1 \int_0^1 dx_2 \delta(\hat{s} + \hat{t} + \hat{u}) G_{\bar{q}/M}(x_1, Q_1^2) G_{q/p}(x_2, Q_2^2) \frac{\hat{s}}{\pi} \frac{d\sigma}{d\hat{t}}(q\bar{q} \rightarrow g\gamma), \quad (2.14)$$

where

$$\hat{s} = x_1 x_2 s, \quad \hat{t} = x_1 t, \quad \hat{u} = x_2 u.$$

Finally, leading-twist contribution to the large- p_T gluon production cross section in the process $\pi p \rightarrow gX$ is

$$\Sigma_M^{LT} \equiv E \frac{d\sigma}{d^3p}(\pi p \rightarrow gX) = \int_0^1 dx_1 \frac{1}{x_1 s + u} G_{\bar{q}/M}(x_1, Q_1^2) G_{q/p}(1 - x_1, Q_2^2) \frac{\hat{s}}{\pi} \frac{d\sigma}{d\hat{t}}(q\bar{q} \rightarrow g\gamma). \quad (2.15)$$

III. HIGHER TWIST MECHANISM WITHIN PERTURBATIVE AND HOLOGRAPHIC QCD AND THE ROLE INFRARED RENORMALONS

The main aim in our studying are the calculation of integral in (2.5) by the running coupling constant approach for different pion distribution amplitudes and the calculation of the extraction of pure contribution of higher-twist and renormalon effects to the cross section. It should be noted that, in the exclusive processes of the coupling constant α_s runs not only due to loop integration but also because of the integration in the process amplitude over the light-cone momentum fraction of hadron constituents. Therefore, it is worth noting

that, the renormalization scale according to Fig.1 should be chosen equal to $Q_1^2 = (1-x)\hat{s}$, and $Q_2^2 = -x\hat{u}$. The integral in Eq.(2.5) in the framework of the running coupling constant approach takes the form

$$D(\mu_{R_0}^2) = \int_0^1 \frac{\alpha_s^{3/2}(\lambda\mu_{R_0}^2)\Phi_M(x, \mu_F^2)dx}{x(1-x)}. \quad (3.1)$$

The $\alpha_s(\lambda\mu_{R_0}^2)$ has the infrared singularity for $\lambda = 0$ and so the integral (3.1) diverges. Thus for the regularization of the integral, we express the running coupling at scaling variable $\alpha_s(\lambda\mu_{R_0}^2)$ with the aid of the renormalization group equation in terms of the fixed one $\alpha_s(Q^2)$. The solution of renormalization group equation for the running coupling $\alpha \equiv \alpha_s/\pi$ has the form [21]

$$\frac{\alpha(\lambda)}{\alpha} = \left[1 + \alpha \frac{\beta_0}{4} \ln \lambda\right]^{-1}. \quad (3.2)$$

Then, for $\alpha_s(\lambda Q^2)$, we get

$$\alpha(\lambda Q^2) = \frac{\alpha_s}{1 + \ln \lambda/t} \quad (3.3)$$

where $t = 4\pi/\alpha_s(Q^2)\beta_0 = 4/\alpha\beta_0$.

If we insert Eq.(3.3) into Eq.(3.1) then, we obtain

$$\begin{aligned} D(\hat{s}, \hat{u}) &= \int_0^1 dx \frac{\alpha_s^{3/2}(\lambda\mu_{R_0}^2)\Phi_M(x, Q_1^2)}{x(1-x)} + \int_0^1 dx \frac{\alpha_s^{3/2}(\lambda\mu_{R_0}^2)\Phi_M(x, Q_2^2)}{x(1-x)} \\ &= \alpha_s^{3/2}(\hat{s})t_1^{3/2} \int_0^1 dx \frac{\Phi_M(x, Q_1^2)}{x(1-x)(t_1 + \ln \lambda_1)^{3/2}} + \alpha_s^{3/2}(-\hat{u})t_2^{3/2} \int_0^1 dx \frac{\Phi_M(x, Q_2^2)}{x(1-x)(t_2 + \ln \lambda_2)^{3/2}} \end{aligned} \quad (3.4)$$

where $t_1 = 4\pi/\alpha_s(\hat{s})\beta_0$ and $t_2 = 4\pi/\alpha_s(-\hat{u})\beta_0$.

Although the integral (3.4) is still divergent, but this expression can be transformed to more useful form as making the change of variable $z = \ln \lambda$, which gives

$$D(\hat{s}, \hat{u}) = \alpha_s^{3/2}(\hat{s})t_1^{3/2} \int_0^1 \frac{\Phi_M(x, Q_1^2)dx}{x(1-x)(t_1 + z_1)^{3/2}} + \alpha_s^{3/2}(-\hat{u})t_2^{3/2} \int_0^1 \frac{\Phi_M(x, Q_2^2)dx}{x(1-x)(t_2 + z_2)^{3/2}}. \quad (3.5)$$

After applying the integral representation of $1/(t+z)^\nu$ [34, 35], we can calculate (3.5),

$$\frac{1}{(t+z)^\nu} = \frac{1}{\Gamma(\nu)} \int_0^\infty e^{-(t+z)u} u^{\nu-1} du, \text{ } Re \nu > 0 \quad (3.6)$$

gives

$$\begin{aligned} D(\hat{s}, \hat{u}) &= \frac{\alpha_s^{3/2}(-\hat{s})t_1^{3/2}}{\Gamma(\frac{3}{2})} \int_0^1 \int_0^\infty \frac{\Phi_\pi(x, Q_1^2)e^{-(t_1+z_1)u} u^{1/2} du dx}{x(1-x)} + \\ &+ \frac{\alpha_s^{3/2}(-\hat{u})t_2^{3/2}}{\Gamma(\frac{3}{2})} \int_0^1 \int_0^\infty \frac{\Phi_\pi(x, Q_2^2)e^{-(t_2+z_2)u} u^{1/2} du dx}{x(1-x)}, \end{aligned} \quad (3.7)$$

For $\Phi^{hol}(x)$ the Eq.(3.7) is written as

$$D(\hat{s}, \hat{u}) = \frac{32\sqrt{\pi}f_\pi}{\beta_0\sqrt{3}\beta_0\Gamma(\frac{3}{2})} \int_0^\infty du e^{-t_1 u} u^{1/2} B\left(\frac{1}{2}, \frac{1}{2} - u\right) + \frac{32\sqrt{\pi}f_\pi}{\beta_0\sqrt{3}\beta_0\Gamma(\frac{3}{2})} \int_0^\infty du e^{-t_2 u} u^{1/2} B\left(\frac{1}{2}, \frac{1}{2} - u\right) \quad (3.8)$$

and for $\Phi_{asy}(x)$ distribution amplitude

$$D(\hat{s}, \hat{u}) = \frac{8\pi\sqrt{3\pi}f_\pi}{\beta_0\sqrt{\beta_0}\Gamma(\frac{3}{2})} \int_0^\infty du e^{-t_1 u} \left[\frac{u^{1/2}}{1-u} \right] + \frac{8\pi\sqrt{3\pi}f_\pi}{\beta_0\sqrt{\beta_0}\Gamma(\frac{3}{2})} \int_0^\infty du e^{-t_2 u} \left[\frac{u^{1/2}}{1-u} \right]. \quad (3.9)$$

and for $\Phi_{CZ}(x, Q^2)$ distribution amplitude

$$D(\hat{s}, \hat{u}) = \frac{8\pi\sqrt{3\pi}f_\pi}{\beta_0\sqrt{\beta_0}\Gamma(\frac{3}{2})} \int_0^\infty du e^{-t_1 u} u^{1/2} \times \left[\frac{1}{1-u} + 0.84 \left[\frac{4}{1-u} - \frac{20}{2-u} + \frac{20}{3-u} \right] \left(\frac{\alpha_s(Q_1^2)}{\alpha_s(\mu_0^2)} \right)^{\frac{50}{81}} \right] + \frac{8\pi\sqrt{3\pi}f_\pi}{\beta_0\sqrt{\beta_0}\Gamma(\frac{3}{2})} \int_0^\infty du e^{-t_2 u} u^{1/2} \left[\frac{1}{1-u} + 0.84 \left[\frac{4}{1-u} - \frac{20}{2-u} + \frac{20}{3-u} \right] \left(\frac{\alpha_s(Q_2^2)}{\alpha_s(\mu_0^2)} \right)^{\frac{50}{81}} \right]. \quad (3.10)$$

and for $\Phi_{BMS}(x, Q^2)$ distribution amplitude

$$D(\hat{s}, \hat{u}) = \frac{8\pi\sqrt{3\pi}f_\pi}{\beta_0\sqrt{\beta_0}\Gamma(\frac{3}{2})} \int_0^\infty du e^{-t_1 u} u^{1/2} \times \left[\frac{1}{1-u} + 0.84 \left[\frac{4}{1-u} - \frac{20}{2-u} + \frac{20}{3-u} \right] \left(\frac{\alpha_s(Q_1^2)}{\alpha_s(\mu_0^2)} \right)^{\frac{50}{81}} \right] + \frac{8\pi\sqrt{3\pi}f_\pi}{\beta_0\sqrt{\beta_0}\Gamma(\frac{3}{2})} \int_0^\infty du e^{-t_2 u} u^{1/2} \left[\frac{1}{1-u} + 0.84 \left[\frac{4}{1-u} - \frac{20}{2-u} + \frac{20}{3-u} \right] \left(\frac{\alpha_s(Q_2^2)}{\alpha_s(\mu_0^2)} \right)^{\frac{50}{81}} \right]. \quad (3.11)$$

where $B(\alpha, \beta)$ is Beta function and u is Borel parameter. The structure of the infrared renormalon poles in Eqs.(3.8) - (3.11) strongly depend on the distributions amplitudes of the pion. To remove them from Eqs.(3.8) - (3.11) we adopt the principal value prescription. In the calculation and figures the higher-twist cross sections obtained using the running coupling and frozen coupling constant approaches are denoted by $(\Sigma_g^{HT})^{res}$ and $(\Sigma_g^{HT})^0$

IV. NUMERICAL RESULTS AND DISCUSSION

We discuss the numerical results for higher-twist and renormalon mechanism with higher-twist contributions calculated in the context of the running and frozen coupling constant

approaches on the dependence of the chosen pion distribution amplitudes in the inclusive gluon production process, $\pi p \rightarrow gX$. For the numerical calculations, for $\pi^+ p \rightarrow gX$ process, we take subprocess as $\pi^+ d_p \rightarrow gu$, in case $\pi^- p \rightarrow gX$, we take subprocess as $\pi^- u_p \rightarrow gd$.

Inclusive gluon production represents a significant test case in which higher-twist terms dominate those of leading-twist in certain kinematic domains. For the dominant leading-twist subprocess for the gluon production, we take the quark-antiquark annihilation $q\bar{q} \rightarrow \gamma g$. In the numerical calculations, for the quark distribution functions inside the pion and proton used as given in [36, 37], respectively.

Obtained results are visualized in Figs. 2-21. In all figures we represent the choice of pion distribution amplitudes Eqs.(2.6) - (2.11) by different line types: $\Phi_{asy}(x)$ as solid black line, $\Phi^{hol}(x)$ as dashed red line, $\Phi_{VSBGL}^{hol}(x)$ as dotted blue line, $\Phi_{CZ}(x, Q^2)$ as dash-dot magenta line, $\Phi_{BMS}(x, Q^2)$ as dash-double dot olive line, and $\Phi_{BELLE}(x, Q^2)$ as short dash navy line. Firstly, it is very interesting comparing the higher-twist cross sections obtained within holographic QCD with the ones obtained within perturbative QCD and also with leading-twist cross section. In Fig.2 and Fig.3 we show the dependence of higher-twist cross sections $(\Sigma_g^{HT})^0, (\Sigma_g^{HT})^{res}$ calculated in the context of the frozen (frozen cross section) and running coupling constant(resummed cross section) approaches as a function of the gluon transverse momentum p_T for the pion distribution amplitudes presented in Eqs.(2.6) - (2.11) at $y = 0$. It is seen from Fig.2 and Fig.3 that the higher-twist cross section is monotonically decreasing with an increase in the transverse momentum of the gluon. In the region $2 \text{ GeV}/c < p_T < 30 \text{ GeV}/c$ the resummed cross sections of the process $\pi^+ p \rightarrow gX$ decreases in the range between $3,172 \cdot 10^{-6} \mu b/\text{GeV}^2$ to $4,912 \cdot 10^{-16} \mu b/\text{GeV}^2$.

In Fig.4 - Fig.6, we show the dependence of the ratios $(\Sigma_g^{HT})^{res}/(\Sigma_g^{HT})^0, (\Sigma_g^{HT})^0/(\Sigma_g^{LT})$ and $(\Sigma_g^{HT})^{res}/(\Sigma_g^{LT})$ in the process $\pi^+ p \rightarrow gX$ which are displayed as a function of p_T for the pion distribution amplitudes presented in Eqs.(2.6)-(2.11) at $y = 0$. As shown in Fig.4, in the region $15 \text{ GeV}/c < p_T < 22 \text{ GeV}/c$, ratio $(\Sigma_g^{HT})^{res}/(\Sigma_g^{HT})^0$ for $\Phi_{CZ}(x, Q^2)$ is enhanced by about two orders of magnitude relative for $\Phi_{asy}(x)$. However, it is one order for $\Phi^{hol}(x)$ and half order for $\Phi_{BMS}(x, Q^2)$ and $\Phi_{BELLE}(x, Q^2)$ pion distribution amplitudes. In Fig.5 and Fig.6, we show the dependence of the ratios $(\Sigma_g^{HT})^0/(\Sigma_g^{LT})$ and $(\Sigma_g^{HT})^{res}/(\Sigma_g^{LT})$, as a function of p_T for the $\Phi^{hol}(x)$, $\Phi_{asy}(x)$ and $\Phi_{VSBGL}^{hol}(x)$ and $\Phi_{CZ}(x, Q^2)$ pion distribution amplitudes. It is seen that in the region $10 \text{ GeV}/c < p_T < 25 \text{ GeV}/c$ leading-twist cross sections is enhanced by about four orders of magnitude relative to the higher-twist cross

sections calculated by frozen coupling constant approach, but in some regions about three orders is suppress of magnitude relative resummed higher-twist cross section for $\Phi_{CZ}(x, Q^2)$. In Fig.7 - Fig.10, we have depicted higher-twist cross sections $(\Sigma_g^{HT})^0$, $(\Sigma_g^{HT})^{res}$ and ratios $(\Sigma_g^{HT})^{res}/(\Sigma_g^{HT})^0$, $(\Sigma_g^{HT})^0/(\Sigma_g^{LT})$ and $(\Sigma_g^{HT})^{res}/(\Sigma_g^{LT})$ as a function of p_T at $\sqrt{s} = 62.4 \text{ GeV}$ for the process $\pi^- p \rightarrow gX$. In Fig.7 and Fig.8 we display the dependence of higher-twist cross sections $(\Sigma_g^{HT})^0$, $(\Sigma_g^{HT})^{res}$ as a function of p_T for the pion distribution amplitudes presented in Eqs.(2.6)-(2.11) at $y = 0$. From the figures we have seen that the higher-twist cross section is monotonically decreasing with an increase in p_T . In this process in the region $2 \text{ GeV}/c < p_T < 30 \text{ GeV}/c$ the resummed cross sections decreases in the range between $4.556 \cdot 10^{-6} \mu b/\text{GeV}^2$ to $6.056 \cdot 10^{-14} \mu b/\text{GeV}^2$. In Fig.9 and Fig.10, we display the dependence of the ratios $(\Sigma_g^{HT})^0/(\Sigma_g^{LT})$ and $(\Sigma_g^{HT})^{res}/(\Sigma_g^{LT})$ in the process $\pi^- p \rightarrow gX$ as a function of p_T for the pion distribution amplitudes presented in Eqs.(2.6)-(2.11) at $y = 0$. It should be noted, that ratio $(\Sigma_g^{HT})^{res}/(\Sigma_g^{HT})^0$ for the $\pi^+ p \rightarrow gX$ process is identical to the ratio $(\Sigma_g^{HT})^{res}/(\Sigma_g^{HT})^0$ for the process $\pi^- p \rightarrow gX$. In Fig.10 we show the dependence of the ratio $(\Sigma_g^{HT})^{res}/(\Sigma_g^{LT})$, as a function of p_T for the pion distribution amplitudes presented in Eqs.(2.6)-(2.11) at $y = 0$. It is also seen from the figure that in the region $10 \text{ GeV}/c < p_T < 30 \text{ GeV}/c$, leading-twist cross sections is enhanced by about three orders of magnitude relative to the frozen cross sections for $\Phi^{hol}(x)$, $\Phi_{asy}(x)$, $\Phi_{CZ}(x, Q^2)$, $\Phi_{BMS}(x, Q^2)$ and $\Phi_{BELLE}(x, Q^2)$ at $y = 0$. But about 4 orders is enhanced by about of magnitude relative to the frozen cross section for $\Phi_{VSBGL}^{hol}(x)$ distribution amplitude, respectively.

Through Fig.11 to Fig.17 the dependence of higher-twist cross sections $(\Sigma_g^{HT})^0$, $(\Sigma_g^{HT})^{res}$, ratios $(\Sigma_g^{HT})^{res}/(\Sigma_g^{HT})^0$, and $(\Sigma_g^{HT})^{res}/(\Sigma_g^{LT})$ are shown in the processes $\pi^+ p \rightarrow \gamma X$ and $\pi^- p \rightarrow \gamma X$ as a function of the y rapidity of the gluon at the transverse momentum of the gluon $p_T = 4.9 \text{ GeV}/c$. It is seen from figures in Fig.11 and Fig.12, frozen and resummed cross sections for all distribution amplitudes of pion has a two maximums where first maximum approximately at the point $y = -2$ and second maximum approximately at the point $y = 2$. Also, leading-twist cross section in $y = 1.5$ has a maximums. Notice that frozen and resummed cross sections for $\Phi_{CZ}(x, Q^2)$ distribution amplitude is enhanced by about half and two orders of magnitude relative to all other distribution amplitudes. In Fig.14- Fig17, we can see that, the dependence of higher-twist cross sections $(\Sigma_g^{HT})^0$, $(\Sigma_g^{HT})^{res}$, ratios $(\Sigma_g^{HT})^{re}/(\Sigma_g^{HT})^0$, and $(\Sigma_g^{HT})^{res}/(\Sigma_g^{LT})$ in the processes $\pi^+ p \rightarrow gX$ and $\pi^- p \rightarrow gX$

are displayed as a function of the y rapidity of the gluon at $p_T = 4.9 \text{ GeV}/c$. Angular distributions the higher-twist cross sections $(\Sigma_g^{HT})^0$, $(\Sigma_g^{HT})^{res}$ for processes $\pi^\pm p \rightarrow \gamma X$ are presented in Figs.18-21. As is seen from the figures cross sections very slowly and smoothly depend of the angle of the scattering. But, angular distributions very sensitive choosing the pion distribution amplitudes.

Analysis of our calculations shows that, $(\Sigma_g^{HT})^0$, $(\Sigma_g^{HT})^{res}$, frozen and resummed higher-twist cross sections and ratios sensitive to pion distribution amplitudes are predicted holographic and perturbative QCD.

We think that this feature of infrared renormalons may help the explain theoretical interpretations with future experimental data for the direct inclusive gluon production cross section in the pion-proton collisions. Higher-twist cross section obtained in our study should be observable at hadron collider.

V. CONCLUSIONS

In this study the inclusive single gluon production via higher twist mechanism within perturbative and holographic QCD are calculated. For calculation of the cross section, the running and frozen coupling constant approaches are applied and infrared renormalon poles in the cross section expression are revealed. Infrared renormalon induced divergences is regularized by means of the principal value prescription and the Borel sum for the higher twist cross section is found. It is observed that, the resummed higher-twist cross section differs from that found using the frozen coupling approximation, in some region, considerably. The following results can be concluded from the experiments; the higher-twist contributions to single gluon production cross section in the pion-proton collisions have important phenomenological consequences and therefore will be helpful for detailed investigation dynamical properties of nucleon. Also the higher-twist gluon production cross section in the pion-proton collisions depends on the form of the pion distribution amplitudes and may be used for future study. Also the contributions of renormalon effects the dependence pion distribution amplitudes in this process is essential and may help to analyse experimental results. We compared frozen and resummed cross sections of the inclusive gluon production in the processes $\pi^- p \rightarrow gX$ and $\pi^+ p \rightarrow gX$. Our calculations show in both cases, running and frozen coupling constant approaches that the inclusive gluon production cross section in the pro-

cess $\pi^- p \rightarrow gX$ is suppress over the inclusive gluon cross section in the process $\pi^+ p \rightarrow gX$. Notice that, the inclusive gluon production spectrum can be measured with large precision, so results obtained in this study will helpful further tests for hadron dynamics at large p_T . As is seen from Eqs.(2.4,3.7) higher twist-cross sections in both cases are proportional with third order of $\alpha_s(Q^2)$, but the leading-twist is linearly proportional to $\alpha_s(Q^2)$. Therefore their ratios is strongly depend on the $\alpha_s^2(Q^2)$. Further investigations are needed in order to clarify the role of higher-twist effects in QCD. In hadron-hadron collisions, inclusive gluon production at large transverse momentum can serve as a short distance in the probe of the incident hadrons. Especially, the future experimental measurements will provide further tests of the dynamical properties of large- p_T hadron production beyond the leading twist.

Acknowledgments

The authors are indebted to V. M. Braun for discussions about the properties of the pion distributions amplitudes. The work of C.A. is supported by KTU under the research project no. BAP 2013/11641.

-
- [1] S. J. Brodsky, G. L. Lepage, and P. B. Mackenzie, Phys. Rev. D **28**, 228 (1983).
 - [2] F. S. Sadykhov and A. I. Akhmedov, Russ. Phys. J. **38**, 513 (1995).
 - [3] A. I. Ahmadov, I. Boztosun, R. Kh. Muradov, A. Soylyu, and E. A. Dadashov, Int. J. Mod. Phys. E**15**, 1209 (2006).
 - [4] A. I. Ahmadov, I. Boztosun, A. Soylyu, and E. A. Dadashov, Int. J. Mod. Phys. E**17**, 1041 (2008).
 - [5] A. I. Ahmadov, C. Aydin, Sh. M. Nagiyev, A. Hakan Yilmaz, and E. A. Dadashov, Phys. Rev. D**80**, 016003 (2009).
 - [6] A. I. Ahmadov, C. Aydin, E. A. Dadashov, and Sh. M. Nagiyev, Phys. Rev. D**81**, 054016 (2010).
 - [7] A. I. Ahmadov, R. M. Burjaliyev, Int. J. Mod. Phys. E**20**, 1243 (2011).
 - [8] A. I. Ahmadov, Sh. M. Nagiyev, and E. A. Dadashov, Int. J. Mod. Phys. E**21**, 1250014 (2012).

- [9] A. I. Ahmadov, C. Aydin, and F. Keskin, Phys. Rev. D **85**, 034009 (2012).
- [10] A. I. Ahmadov, C. Aydin, and F. Keskin, Ann. Phys. **327**, 1472 (2012).
- [11] A. I. Ahmadov, C. Aydin, and O. Uzun, Phys. Rev. D **87**, 014006 (2013).
- [12] A. I. Ahmadov, C. Aydin, and O. Uzun, Phys. Rev. D **89**, 014018 (2014).
- [13] J. A. Bagger and J. F. Gunion, Phys. Rev. D **29**, 40 (1984).
- [14] A. Bagger and J. F. Gunion, Phys. Rev. D **25**, 2287 (1982).
- [15] V. N. Baier and A. Grozin, Phys. Lett. **96B**, 181 (1980); S. Gupta, Phys. Rev. D **24**, 1169 (1981).
- [16] G.'t. Hooft, in The Whys of Subnuclear Physics, Erice, 1977, edited by A. Zichichi (Plenum, New York, 1979), p.94
- [17] A. H. Mueller, Nucl. Phys. **B 250**, 327 (1985); Phys. Lett. **B 308**, 355 (1993).
- [18] V. I. Zakharov, Nucl. Phys. **B 385**, 452 (1992).
- [19] M. Beneke, Phys. Rep. **317**, 1 (1999).
- [20] W. Greiner, S. Schramm and E. Stein, Quantum Chromodynamics, 3rd edn.(Berlin, Springer, 2007), pp.553.
- [21] H. Contopanagos and G. Sterman, Nucl. Phys. **B 419**, 77 (1994).
- [22] S. S. Agaev, Phys. Lett. **B 360**, 117 (1995); **B 369**, 379(E) (1996).
- [23] G. L. Lepage and S. J. Brodsky, Phys. Rev. D **22**, 2157 (1980).
- [24] J.F. Owens, Rev. Modern Phys. **59**, 465 (1987).
- [25] E. L. Berger and S. J. Brodsky, Phys. Rev. D **24**, 2428 (1981).
- [26] G. P. Lepage and S. J. Brodsky, Phys. Lett. **87B**, 359 (1979).
- [27] A. Vega, I. Schmidt, T. Branz, T. Gutsche, V. Lyubovitskij, Phys. Rev. D **80**, 055014 (2009).
- [28] S. J. Brodsky and G. F. de Teramond, Phys. Rev. D **77**, 056007 (2008).
- [29] S. J. Brodsky, Proc. Sci., LHC07 (2007) 002.
- [30] V. L. Chernyak and A. R. Zhitnitsky, Phys. Rep. **112**, 173 (1984).
- [31] A. P. Bakulev, S. V. Mikhailov and N. G. Stefanis, Phys. Lett, **B 578**, 91 (2004); A. P. Bakulev, S.V. Mikhailov, A.V. Pimikov, and N. G. Stefanis, Phys. Rev. D **86**, 031501 (2012).
- [32] S. Uehara et al. [Belle Collaboration], Phys. Rev. D **86**, 092007 (2012)..
- [33] E. L. Berger, Phys. Rev. D **26**, 105 (1982).
- [34] J. Zinn-Justin, Phys. Rept. **70**, 109 (1981).
- [35] A. Erdelyi, Higher Transcendental Functions (McGraw-Hill Book Company, New York, 1953),

Vol.2.

- [36] S.-i Nam, Phys. Rev. D**86**, 074005 (2012).
- [37] A.D. Martin, W. J. Stirling, R.S. Thorne, G. Watt, Eur. Phys. J. C**63**, 189 (2009).

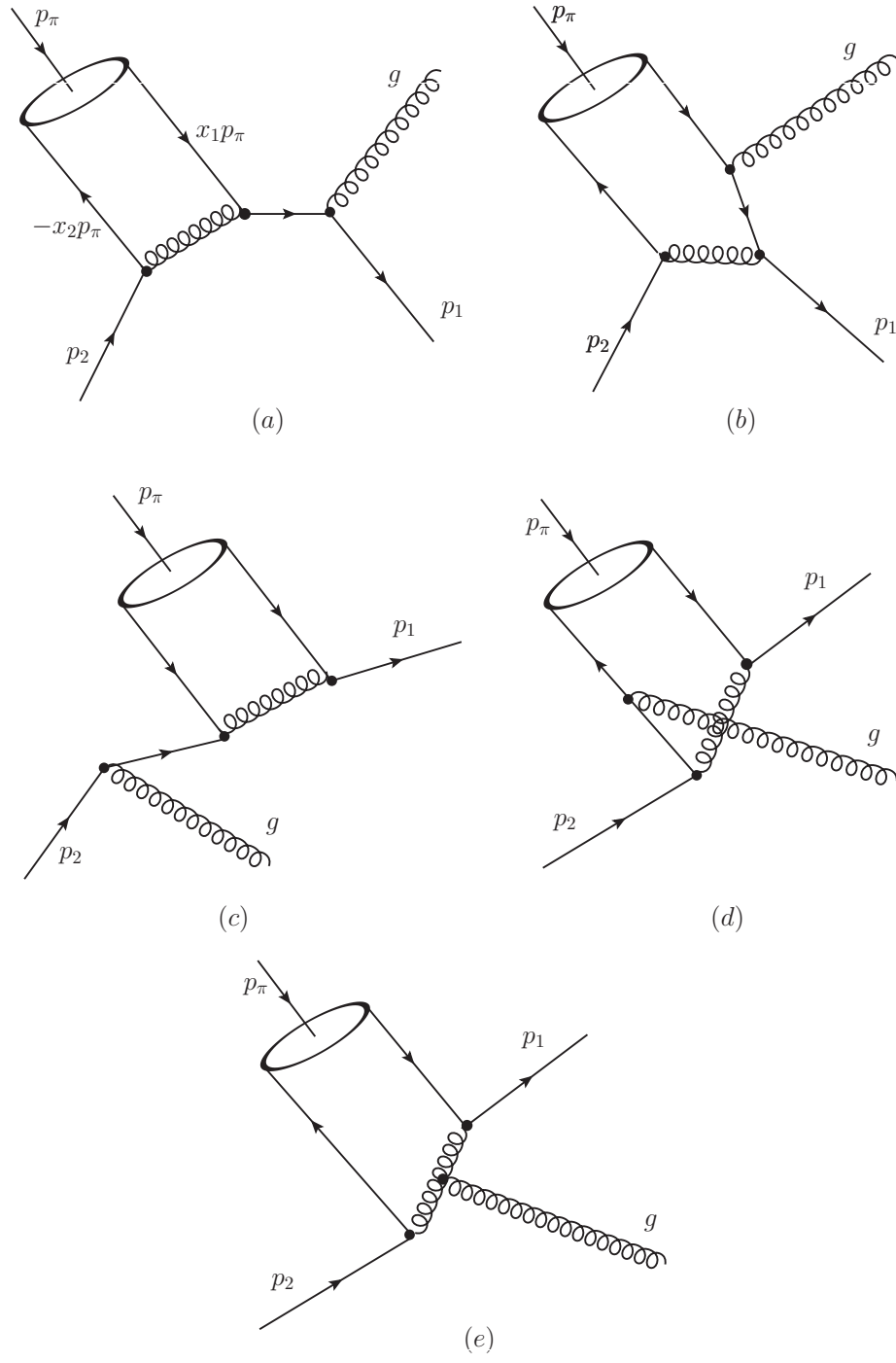


FIG. 1: Full set of QCD Feynman diagrams for higher-twist subprocess $\pi q \rightarrow gq$.

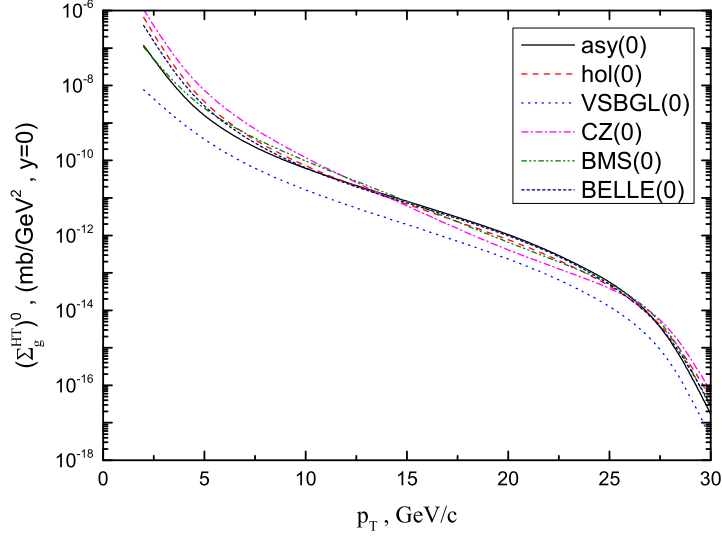


FIG. 2: Higher-twist $\pi^+p \rightarrow gX$ inclusive gluon production cross section $(\Sigma_g^{HT})^0$ as a function of the p_T transverse momentum of the gluon at the c.m. energy $\sqrt{s} = 62.4 \text{ GeV}$.

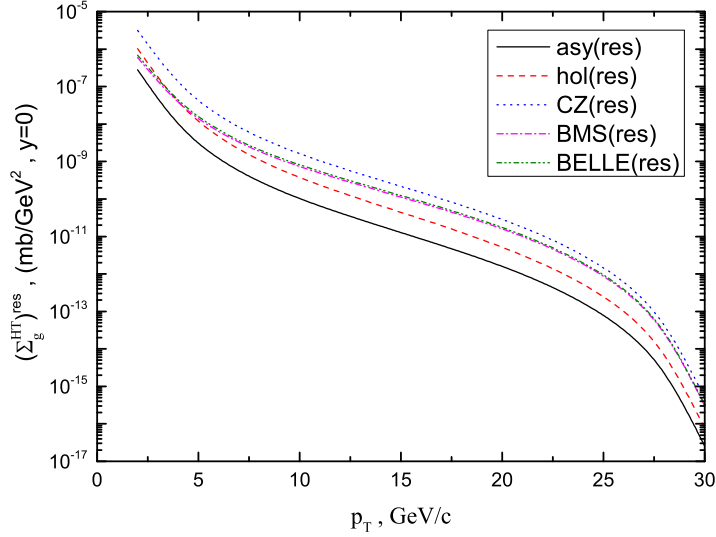


FIG. 3: Higher-twist $\pi^+p \rightarrow gX$ inclusive gluon production cross section $(\Sigma_g^{HT})^{res}$ as a function of the p_T transverse momentum of the gluon at the c.m. energy $\sqrt{s} = 62.4 \text{ GeV}$.

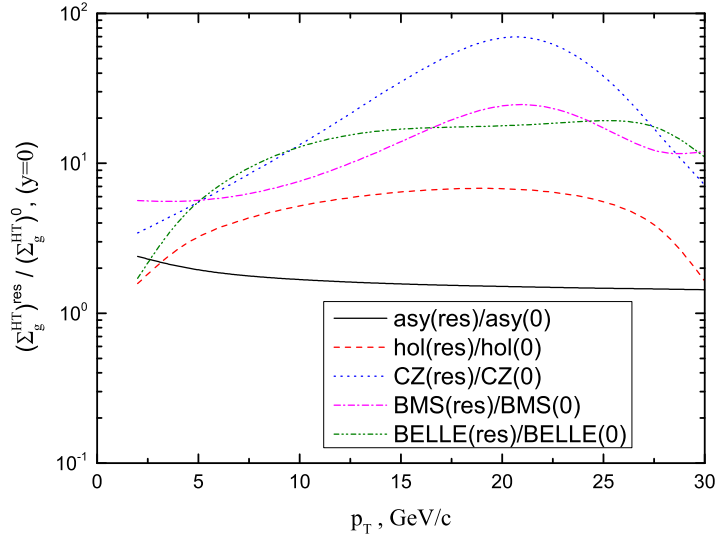


FIG. 4: Ratio $(\Sigma_g^{HT})^{res}/(\Sigma_g^{HT})^0$, in the process $\pi^+p \rightarrow gX$, where higher-twist contribution are calculated for the gluon rapidity $y = 0$ at the c.m.energy $\sqrt{s} = 62.4 \text{ GeV}$ as a function of the gluon transverse momentum, p_T .

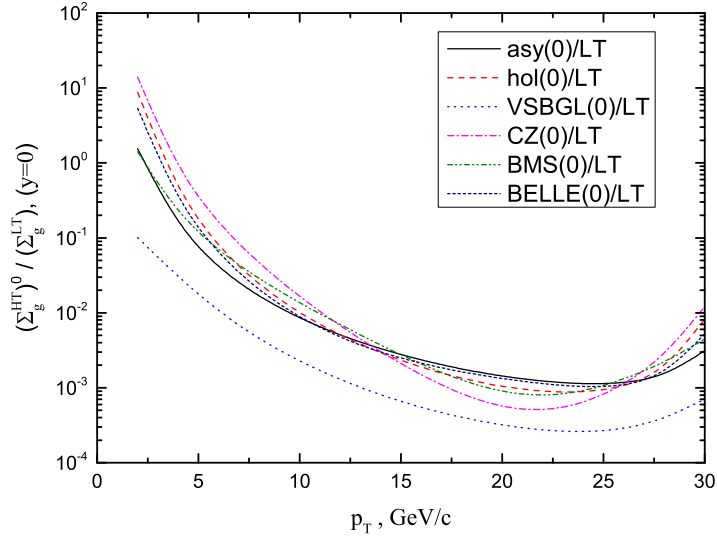


FIG. 5: Ratio $(\Sigma_g^{HT})^0/(\Sigma_g^{LT})$, in the process $\pi^+p \rightarrow gX$, as a function of the p_T transverse momentum of the gluon at the c.m. energy $\sqrt{s} = 62.4 \text{ GeV}$.

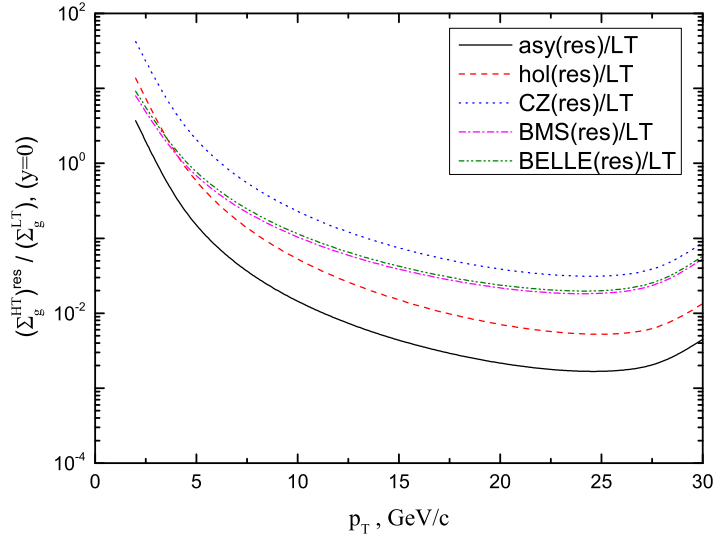


FIG. 6: Ratio $(\Sigma_g^{HT})^{res}/(\Sigma_g^{LT})$, in the process $\pi^+p \rightarrow gX$, as a function of the p_T transverse momentum of the gluon at the c.m. energy $\sqrt{s} = 62.4 \text{ GeV}$.

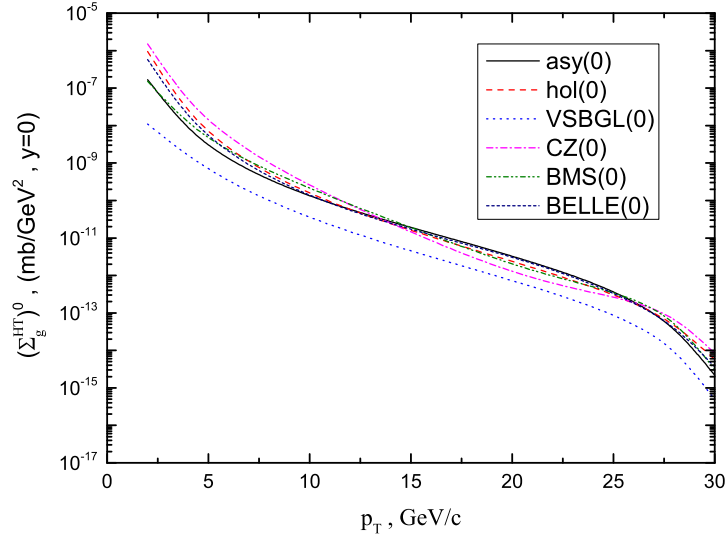


FIG. 7: Higher-twist $\pi^-p \rightarrow gX$ inclusive gluon production cross section $(\Sigma_g^{HT})^0$ as a function of the p_T transverse momentum of the gluon at the c.m. energy $\sqrt{s} = 62.4 \text{ GeV}$.

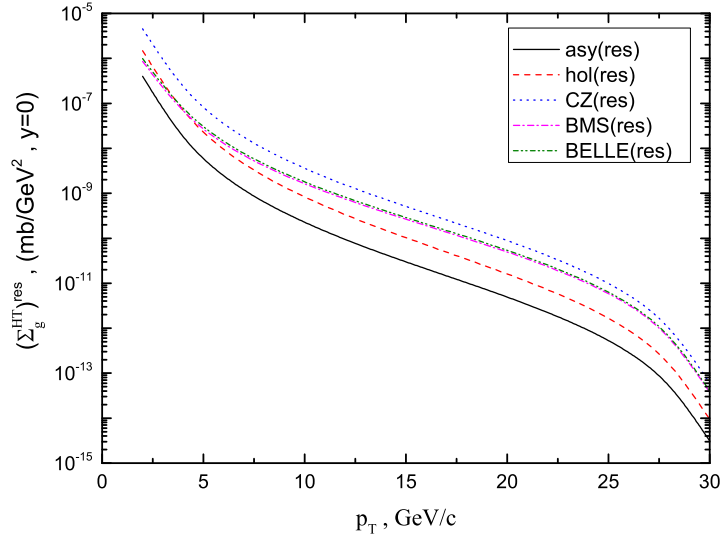


FIG. 8: Higher-twist $\pi^-p \rightarrow gX$ inclusive gluon production cross section $(\Sigma_g^{HT})^{res}$ as a function of the p_T transverse momentum of the gluon at the c.m.energy $\sqrt{s} = 62.4 \text{ GeV}$.

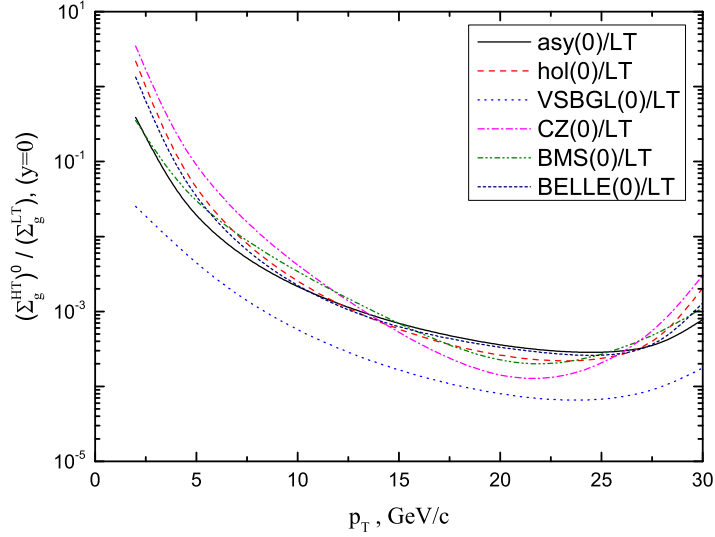


FIG. 9: Ratio $(\Sigma_g^{HT})^0 / (\Sigma_g^{LT})$, in the process $\pi^-p \rightarrow gX$, as a function of the p_T transverse momentum of the gluon at the c.m. energy $\sqrt{s} = 62.4 \text{ GeV}$.

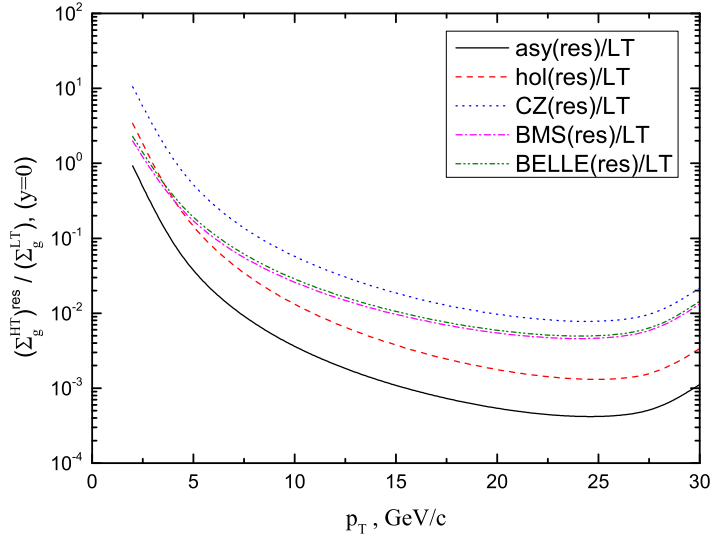


FIG. 10: Ratio $(\Sigma_g^{HT})^{res}/(\Sigma_g^{LT})$, in the process $\pi^-p \rightarrow gX$, as a function of the p_T transverse momentum of the gluon at the c.m. energy $\sqrt{s} = 62.4 \text{ GeV}$.

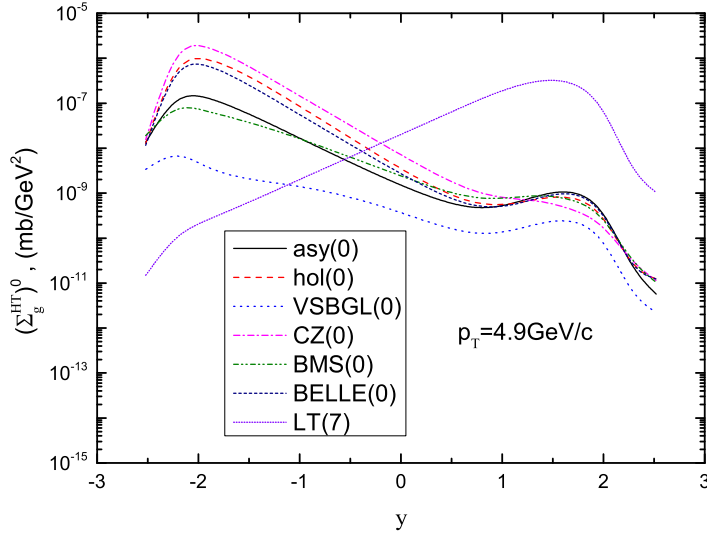


FIG. 11: Higher-twist $\pi^+p \rightarrow gX$ inclusive gluon production cross section $(\Sigma_g^{HT})^0$, as a function of the y rapidity of the gluon at the transverse momentum of the gluon $p_T = 4.9 \text{ GeV}/c$, at the c.m. energy $\sqrt{s} = 62.4 \text{ GeV}$.

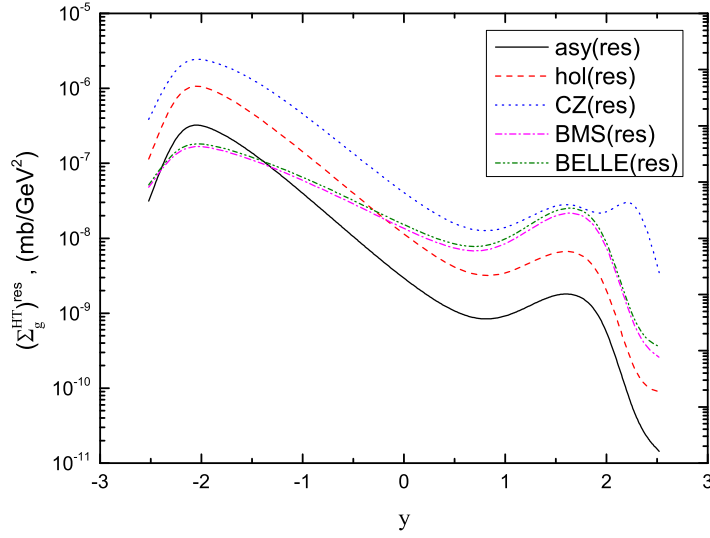


FIG. 12: Higher-twist $\pi^+p \rightarrow gX$ inclusive gluon production cross section $(\Sigma_g^{HT})^{res}$, as a function of the y rapidity of the gluon at the transverse momentum of the gluon $p_T = 4.9 \text{ GeV}/c$, at the c.m. energy $\sqrt{s} = 62.4 \text{ GeV}$.

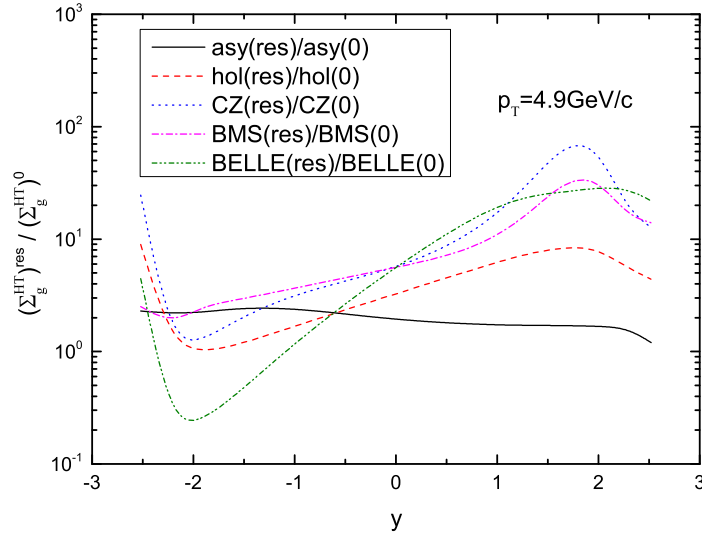


FIG. 13: Ratio $(\Sigma_g^{HT})^{res}/(\Sigma_g^{HT})^0$, in the process $\pi^-p \rightarrow gX$, as a function of the y rapidity of the gluon at the transverse momentum of the gluon $p_T = 4.9 \text{ GeV}/c$, at the c.m. energy $\sqrt{s} = 62.4 \text{ GeV}$.

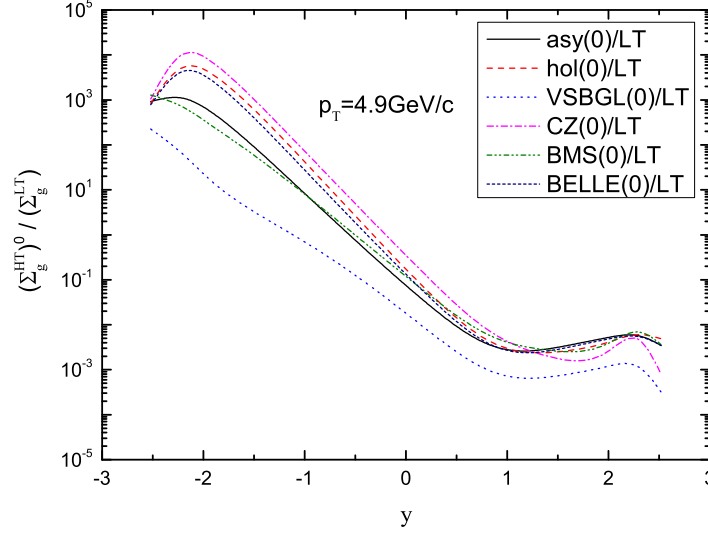


FIG. 14: Ratio $(\Sigma_g^{HT})^0/(\Sigma_g^{LT})$ in the process $\pi^+p \rightarrow gX$, as a function of the y rapidity of the gluon at the transverse momentum of the gluon $p_T = 4.9 \text{ GeV}/c$, at the c.m. energy $\sqrt{s} = 62.4 \text{ GeV}$.

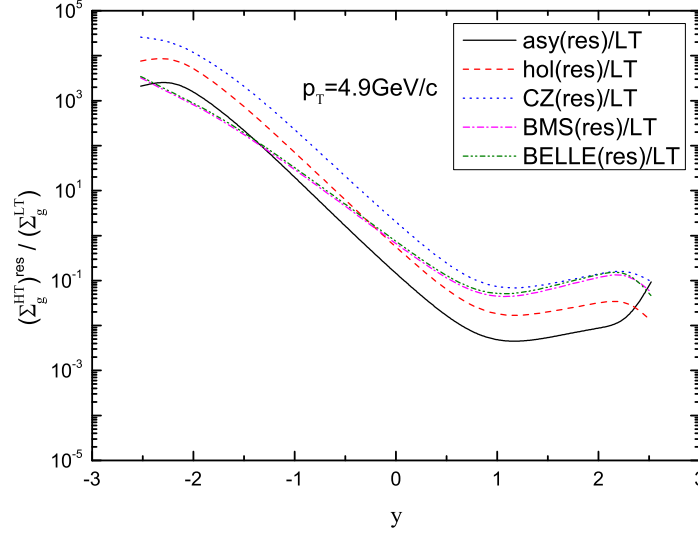


FIG. 15: Ratio $(\Sigma_g^{HT})^{res}/(\Sigma_g^{LT})$ in the process $\pi^+p \rightarrow gX$, as a function of the y rapidity of the gluon at the transverse momentum of the gluon $p_T = 4.9 \text{ GeV}/c$, at the c.m. energy $\sqrt{s} = 62.4 \text{ GeV}$.

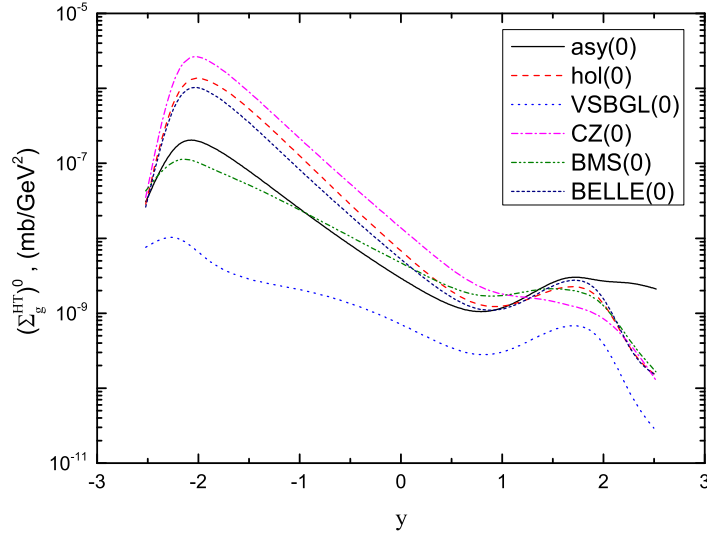


FIG. 16: Higher-twist $\pi^- p \rightarrow gX$ inclusive gluon production cross section $(\Sigma_g^{HT})^0$, as a function of the y rapidity of the gluon at the transverse momentum of the gluon $p_T = 4.9 \text{ GeV}/c$, at the c.m. energy $\sqrt{s} = 62.4 \text{ GeV}$.

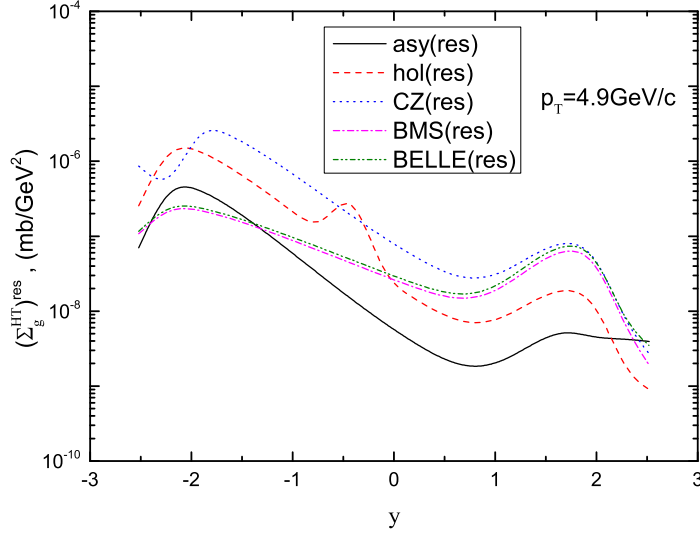


FIG. 17: Higher-twist $\pi^- p \rightarrow gX$ inclusive gluon production cross section $(\Sigma_g^{HT})^{res}$, as a function of the y rapidity of the gluon at the transverse momentum of the gluon $p_T = 4.9 \text{ GeV}/c$, at the c.m. energy $\sqrt{s} = 62.4 \text{ GeV}$.

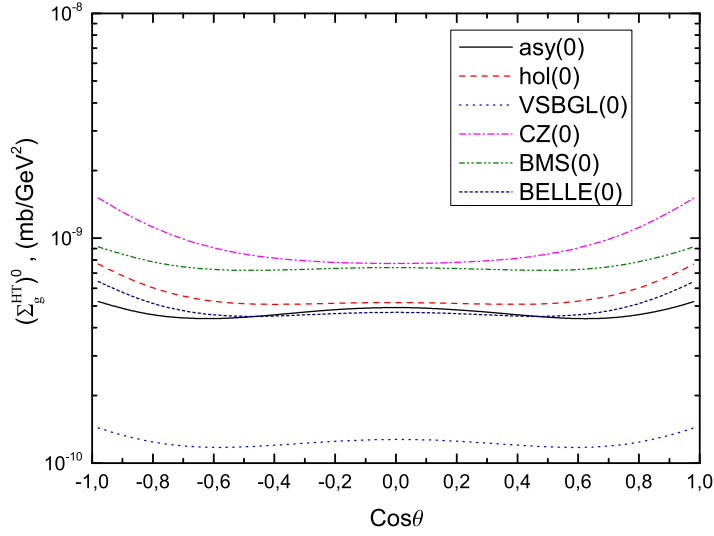


FIG. 18: Angular distribution higher-twist cross section $(\Sigma_g^{HT})^0$ in the process $\pi^+p \rightarrow gX$, at the transverse momentum of the gluon $p_T = 4.9 \text{ GeV}/c$, at the c.m. energy $\sqrt{s} = 62.4 \text{ GeV}$.

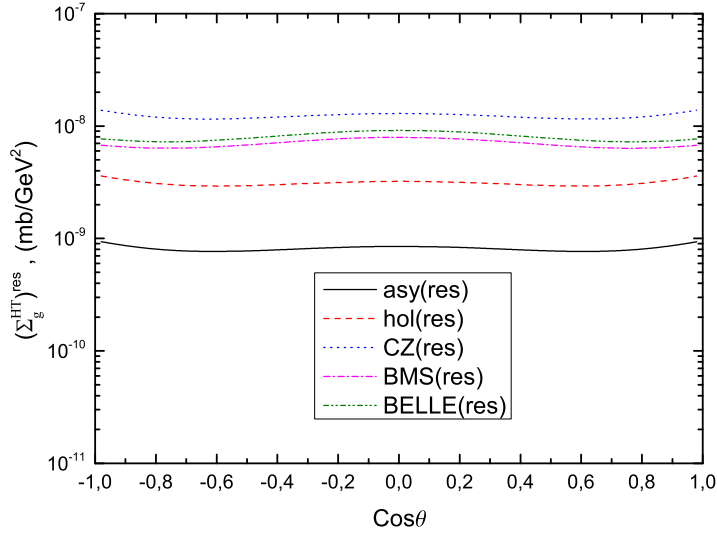


FIG. 19: Angular distribution higher-twist cross section $(\Sigma_g^{HT})^{res}$ in the process $\pi^+p \rightarrow gX$, at the transverse momentum of the gluon $p_T = 4.9 \text{ GeV}/c$, at the c.m. energy $\sqrt{s} = 62.4 \text{ GeV}$.

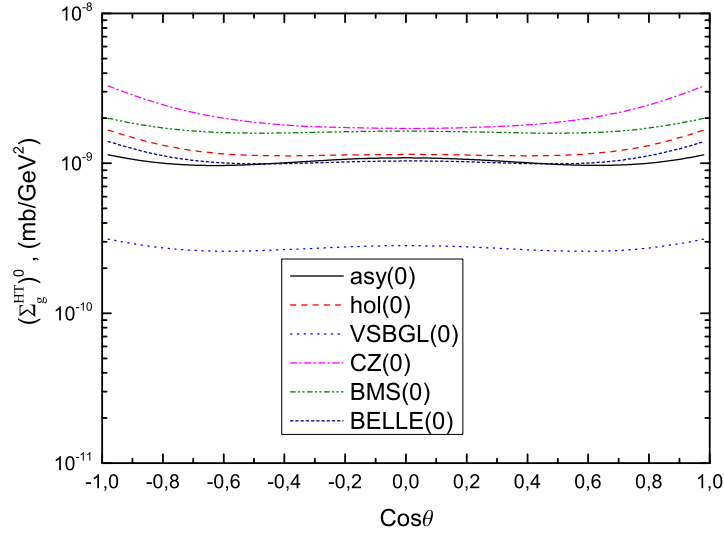


FIG. 20: Angular distribution higher-twist cross section $(\Sigma_g^{HT})^0$ in the process $\pi^- p \rightarrow gX$, at the transverse momentum of the gluon $p_T = 4.9 \text{ GeV}/c$, at the c.m. energy $\sqrt{s} = 62.4 \text{ GeV}$.

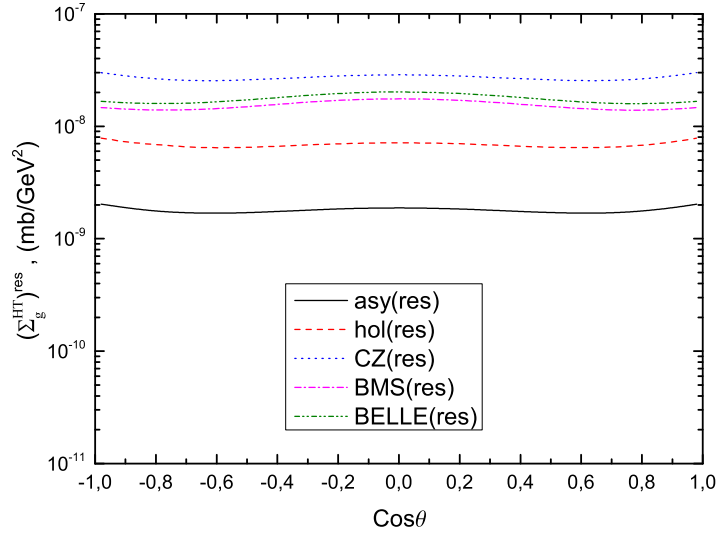


FIG. 21: Angular distribution higher-twist cross section $(\Sigma_g^{HT})^{res}$ in the process $\pi^- p \rightarrow gX$, at the transverse momentum of the gluon $p_T = 4.9 \text{ GeV}/c$, at the c.m. energy $\sqrt{s} = 62.4 \text{ GeV}$.